Mathematical and Computer Modelling of Dynamical Systems
Vol. 11, No. 3, September 2005, 255–272

Taylor & Francis
Taylor & Francis Group

Modelling an Inertia Wheel Pendulum Benchmark

DIEGO M. ALONSO*[†,‡], FEDERICO I. ROBBIO[†,‡], EDUARDO E. PAOLINI[†] and JORGE L. MOIOLA[†,‡]

[†]Instituto de Investigaciones en Ingeniería Eléctrica, Depto. de Ingeniería Eléctrica y de Computadoras, Universidad Nacional del Sur, Bahía Blanca, Argentina.
[‡]Consejo Nacional de Investigaciones Científicas y Técnicas (CONICET), Argentina

In this paper, modelling and parameter identification of an inertia wheel pendulum benchmark is considered. This is an underactuated mechanical system useful for teaching and research. Attention is focused on deriving a simple but accurate model capable of reproducing large amplitude oscillations. Due to the particular design of the prototype, the friction forces on the actuated joint are noticeable. A simple friction model including dead-zone effects and viscous terms is proposed, and a compensation method for the dead zone is derived. The accuracy of the compensation strategy and the predictive quality of the derived model are analysed by comparing numerical simulations with experimental data.

Keywords: Underactuated mechanical systems, non-linear oscillations, static friction, friction compensation

1. Introduction

The techniques for designing controllers for real world applications require appropriate mathematical models to guarantee some desired closed-loop performance. Therefore, modelling and parameter identification methods become important issues for a successful practical implementation of the control strategy. Existing methods range from black-box modelling, when a precise relation between meaningful parameters and measured variables is unknown, to those developed after a careful analysis of the behaviour of the system based, for example, on physical principles. When knowledge of the physical properties of the system is not enough to construct a physically parametrized model, both techniques can be combined leading to a semiphysical or 'grey-box' model [1].

*Corresponding author. Diego M. Alonso, Depto. de Ingeniería Eléctrica y de Computadoras, Universidad Nacional del Sur, Avda. Alem 1253, B8000CPB Bahía Blanca, Argentina. Phone: + 54 291 4595180. Fax: + 54 291 4595154. E-mail: dalonso@criba.edu.ar

Mathematical and Computer Modelling of Dynamical Systems
ISSN 1387-3954 print/ISSN 1744-5051 online © 2005 Taylor & Francis
http://www.tandf.co.uk/journals
DOI: 10.1080/13873950500076784

For mechanical systems, a classical method to derive the equations of motion is the Euler–Lagrange approach (see [2] for a detailed description). As is well known, this approach requires the computation of kinetic and potential energies and knowledge of the forces acting on the system. The latter can be relatively difficult to model and, in general, depend on constructive aspects. For instance, in mechanical systems involving parts in contact with relative motion the presence of friction forces is inevitable [3] and, if neglected when deriving the model, they can deteriorate the performance of control strategies leading to undesirable effects such as stick-slip motion or limit cycling [4–6], positioning or tracking errors, among others. These phenomena are more noticeable at very low velocities, and friction compensation is mandatory when dealing with high precision positioning or tracking tasks. Towards this end, elaborated friction models and friction compensation techniques have been developed in the last few years (see for example [7, 8]).

In this paper, modelling and parameter identification of an actual under-actuated mechanical system is presented. The system, known as the inertia wheel pendulum, consists of a conventional pendulum with a rotating disk at the end; the pendulum can rotate freely while the disk is driven by a dc motor. The prototype uses a small, inexpensive dc motor coupled to the disk by a rubber belt that amplifies the applied torque, but also increases considerably the friction at the bearings. The motor–disk subsystem is subject to a simple but accurate friction compensation scheme, simplifying the mathematical description and yielding an almost 'ideal model'. Attention is focused on obtaining a model valid for the analysis of large amplitude oscillations. Since they can be associated with a relatively high disk velocity, the performance of the compensator is not analysed at low velocities. To evaluate the accuracy of the identified model, large amplitude oscillations are generated using a state feedback controller, and simulations are compared with experimental data. The studied system constitutes an interesting benchmark for introducing undergraduate students to control methodologies and the problems arising in their practical implementation, and also for testing more advanced control strategies such as non-linear stabilizing controllers [9–14] or amplitude control of oscillations [15].

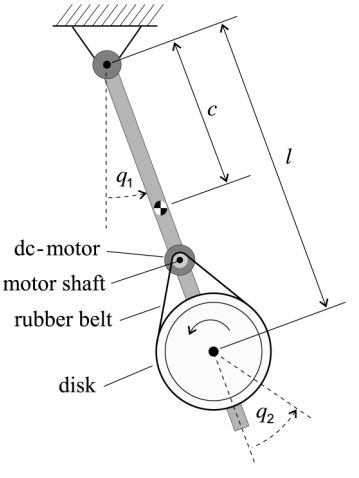

Figure 1. The inertia wheel pendulum.

2. Equations of motion

The equations of motion of the inertia wheel pendulum (see figure 1) are obtained using the Euler–Lagrange formalism considering as generalized coordinates the angular position of the pendulum (q_1) and the angular position of the disk (q_2) relative to the arm, and computing

$$\frac{d}{dt}\left(\frac{\partial}{\partial \dot{q}} L(q,\dot{q})\right) - \frac{\partial}{\partial q} L(q,\dot{q}) = \tau, \tag{1}$$

where $q = [q_1 \quad q_2]^{\mathrm{T}}$ are generalized coordinates of the system, $L = T - V$ is the Lagrangian, T is the kinetic energy, V is the potential energy and $\tau = [\tau_1 \quad \tau_2]^{\mathrm{T}}$ is the vector of generalized forces acting on the system.

The kinetic energy of the system is

$$T = \frac{1}{2}\left(I_1 + m_1 c^2 + m_2 l^2\right)\dot{q}_1^2 + \frac{1}{2} I_2 \left(\dot{q}_1 + \dot{q}_2\right)^2,$$

and the potential energy is

$$V = (m_1 c + m_2 l) g (1 - \cos q_1),$$

where m_1 and I_1 are the mass and the moment of inertia of the pendulum, m_2 and I_2 are the mass and the moment of inertia of the disk, l and c are the distances from the pivot point to the disk shaft and to the centre of mass of the arm, respectively, and g is the acceleration due to gravity. Then, the Lagrangian is

$$L = \frac{1}{2}\hat{I}_1 \dot{q}_1^2 + \frac{1}{2} I_2 \left(\dot{q}_1 + \dot{q}_2\right)^2 - (m_1 c + m_2 l) g (1 - \cos q_1), \tag{2}$$

where $\hat{I}_1 := I_1 + m_1 c^2 + m_2 l^2$.

A classical model of the torque developed by the dc motor is

$$\tau_m = \frac{k_T}{R} V_i - \frac{k_T k_F}{R} \omega_m,$$

where k_T is the torque constant, R is the rotor coil resistance, V_i is the control voltage, k_F is the back-emf constant, and ω_m is the angular velocity of the motor shaft. The electric time constant of the motor has been neglected since generally it is much smaller than the mechanical time constant. Due to the coupling by the rubber belt, the torque applied to the disk joint is $\tau_{\mathrm{d}} = N\tau_m$ and the angular velocity of the disk is $\dot{q}_2 = 1/N\,\omega_m$, where N is the ratio between the diameter of the inertia disk and the diameter of the motor pulley, known as the reduction ratio. Therefore, the torque applied to the disk is

$$\tau_d = \frac{N k_T}{R} V_i - \frac{N^2 k_T k_F}{R} \dot{q}_2 \,. \tag{3}$$

The equations of motion are obtained computing (1) with (2), giving

$$\left(\hat{I}_1 + I_2\right)\ddot{q}_1 + I_2\ddot{q}_2 + (m_1 c + m_2 l) g \sin q_1 = -\tau_{f1}, \tag{4a}$$

$$I_2\ddot{q}_1 + I_2\ddot{q}_2 = \tau_d - \tau_{f2}, \tag{4b}$$

where τ_{f1} and τ_{f2} are the friction torques at the joints of the pendulum and the disk, respectively. The friction model adopted for τ_{f1} and τ_{f2} is analysed next.

3. Friction torques

Due to the mechanical design of the system the most significative friction effects on each joint are of different natures; therefore both joints are analysed separately. As stated before, attention is focused on deriving the simplest model capable of reproducing oscillations of large amplitude; this dispenses with applying elaborated friction models such as [7] or [8], for example, as the performance of the model at low velocities is not the main topic of study.

3.1 Friction at the Pendulum Joint

Friction forces acting on the pendulum joint comprise viscous friction and rolling friction,

$$\tau_{f1} = \tau_{v1} + \tau_{r1},$$

respectively. When performing large amplitude oscillations, static and Coulomb friction at this joint can be neglected and they are not included in the model.

Viscous friction. The term τ_{v1} takes into account the resistance offered by the air to the pendulum movement and the effect of lubrication at the bearing. Its magnitude is directly proportional to the angular velocity of the pendulum, and it is modelled as

$$\tau_{v1} = \sigma_{v1}\dot{q}_1,$$

where σ_{v1} is a positive real parameter.

Rolling friction. This type of friction occurs at the bearing of the pendulum due to the elastic deformation of the shaft caused by the pendulum load. The friction torque is

$$\tau_{r1} = \mu_r F r,$$

where μ_r is the friction coefficient, F is the normal contact force and r is the radius of the pendulum shaft. In general, the coefficient μ_r is not constant [3], and may depend on velocity, among other factors. As will be shown later, a linear dependency with the shaft speed ($\mu_r = \sigma_r \dot{q}_1$, $\sigma_r > 0$) leads to a fairly approximate model. Providing that $r \ll l$ and $r \ll c$, the normal contact force results in

$$F = (m_1 + m_2) g |\cos q_1| + (m_1 c + m_2 l)\dot{q}_1^2,$$

where the first term represents the effect of gravity, and the second term accounts for the effect of centrifugal force. Then, the rolling friction torque results

$$\tau_{r1} = \sigma_{a1} |\cos q_1| \dot{q}_1 + \sigma_{b1} \dot{q}_1^3,$$

where $\sigma_{a1} := \sigma_r (m_1 + m_2) g r$ and $\sigma_{b1} := \sigma_r (m_1 c + m_2 l) r$.

3.2 Friction at the Disk Joint

Friction forces at the bearings of the motor and disk are greatly increased by the stress imposed by the rubber belt coupling. The main phenomenon at this joint is a dead zone relating the disk velocity with the control input V_i. This non-linear characteristic severely modifies the proposed linear model (3) and can be modelled as a friction torque depending on the control voltage. The friction torque at the disk joint reads

$$\tau_{f2} = \tau_{\mathrm{dz}} + \sigma_{v2} \dot{q}_2,$$

where τ_{dz} accounts for the dead-zone effect, and σ_{v2} is a positive parameter representing the coefficient of an additional viscous friction term. Although a Coulomb friction term $\tau_{\mathrm{cf}} = \sigma_{c2} \operatorname{sgn} \dot{q}_2$, $\sigma_{c2} > 0$, may also be included, it will be shown later that the dynamical behaviour of the motor–disk subsystem can be predicted with acceptable accuracy considering only dead-zone and viscous friction terms.

The dead zone between the disk velocity and the control input V_i is modelled as

$$\tau_{\mathrm{dz}} = \frac{N k_T}{R} f(V_i), \tag{5}$$

with

$$f(V_i) = \begin{cases} V_{\mathrm{dz}}^+, & V_i > V_{\mathrm{dz}}^+, \\ V_i & -V_{\mathrm{dz}}^- < V_i < V_{\mathrm{dz}}^+, \\ -V_{\mathrm{dz}}^-, & V_i < -V_{\mathrm{dz}}^-, \end{cases}$$

where V_{dz}^+ and V_{dz}^- are positive parameters. A simpler model can be obtained letting $V_{\mathrm{dz}}^+ = V_{\mathrm{dz}}^-$, but the former is preferred since the dc motor may present non-symmetrical behaviour depending on the sign of the applied voltage due to the shift of the brushes to reduce the armature reaction effect. A more general model may also use different values for coefficient $N k_T / R$ depending on the sign of V_i.

4. State space model and parameter identification

The state space model of the inertia wheel pendulum is obtained from the equations of motion (4) taking as state variables the angular position and velocity of the pendulum (q_1 and q_3, respectively) and the angular position and velocity of the disk (q_2 and q_4, respectively) and defining the non-dimensional control input $v = V_i / \beta$, where β is a positive parameter that accounts for the gain of the motor driver, among other practical issues. The four-dimensional state space model is then

$$
\begin{aligned}
\dot{q}_1 &= q_3,\\
\dot{q}_2 &= q_4,\\
\dot{q}_3 &= -p_1 \sin q_1 - \tilde{\sigma}_{a1} |\cos q_1| q_3 - \tilde{\sigma}_{v1}\, q_3 - \tilde{\sigma}_{b1}\, q_3^3 + p_2 q_4 + \tilde{\tau}_{\mathrm{dz}} - p_3 v,\\
\dot{q}_4 &= p_1 \sin q_1 + \tilde{\sigma}_{a1} |\cos q_1| q_3 + \tilde{\sigma}_{v1}\, q_3 + \tilde{\sigma}_{b1}\, q_3^3 - p_2(1+\rho) q_4 - (1+\rho)\,\tilde{\tau}_{\mathrm{dz}}\\
&\quad + p_3(1+\rho) v,
\end{aligned}
\tag{6}
$$

where the dead-zone component is redefined as $\tilde{\tau}_{\mathrm{dz}} = \tau_{\mathrm{dz}} / \hat{I}_1$ and the parameters are

$$
p_1 := \frac{(m_1 c + m_2 l) g}{\hat{I}_1}, \quad p_2 := \frac{N^2 k_T k_F}{\hat{I}_1 R} + \frac{\sigma_{v2}}{\hat{I}_1}, \quad p_3 := \frac{\beta N k_T}{\hat{I}_1 R}, \quad \rho := \frac{\hat{I}_1}{I_2},
$$

$$
\tilde{\sigma}_{a1} := \frac{\sigma_{a1}}{\hat{I}_1}, \quad \tilde{\sigma}_{b1} := \frac{\sigma_{b1}}{\hat{I}_1}, \quad \tilde{\sigma}_{v1} := \frac{\sigma_{v1}}{\hat{I}_1}.
$$

As mentioned before, to simplify the model it is convenient to compensate the discontinuous friction component $\tilde{\tau}_{\mathrm{dz}}$ using a feedforward controller. Toward this end, the proposed input is

$$
v = u + \frac{1}{p_3} \tilde{\tau}_c(u), \tag{7}
$$

where u is the ideal input and $\tilde{\tau}_c(u)$ is the dead-zone compensation term given by

$$
\tilde{\tau}_c(u) = \begin{cases} p_3 v^+, & u > 0,\\ 0, & u = 0,\\ -p_3 v^-, & u < 0, \end{cases} \tag{8}
$$

where $v^+ = V_{\mathrm{dz}}^+ / \beta$ and $v^- = V_{\mathrm{dz}}^- / \beta$.

Therefore, the state space model of the feedforward compensated system results in

$$
\begin{aligned}
\dot{q}_1 &= q_3,\\
\dot{q}_2 &= q_4,\\
\dot{q}_3 &= -p_1 \sin q_1 - \tilde{\sigma}_{a1} |\cos q_1| q_3 - \tilde{\sigma}_{v1}\, q_3 - \tilde{\sigma}_{b1}\, q_3^3 + p_2 q_4 - p_3 u,\\
\dot{q}_4 &= p_1 \sin q_1 + \tilde{\sigma}_{a1} |\cos q_1| q_3 + \tilde{\sigma}_{v1}\, q_3 + \tilde{\sigma}_{b1}\, q_3^3 - p_2(1+\rho) q_4 + p_3(1+\rho) u.
\end{aligned}
\tag{9}
$$

The actual value of the model parameters can be obtained by an off-line least square identification procedure. The equations concerning $\dot{q}_3$ and $\dot{q}_4$ can be written exhibiting linear parameter dependency as

$$
\Phi(t)\theta = \phi(t),
$$

where

$$
\phi(t) = [\, \dot{q}_3 \quad \dot{q}_4 \,]^T, \tag{10}
$$

and

$$\Phi(t) = \begin{bmatrix} -\sin q_1 & -|\cos q_1| q_3 & -q_3 & -q_3^3 & q_4 & -u & 0 & 0 \\ \sin q_1 & |\cos q_1| q_3 & q_3 & q_3^3 & 0 & 0 & -q_4 & u \end{bmatrix}, \tag{11}$$

depend on measurable signals, and θ is the vector of unknown parameters given by

$$\theta = [p_1 \quad \tilde{\sigma}_{a1} \quad \tilde{\sigma}_{v1} \quad \tilde{\sigma}_{b1} \quad p_2 \quad p_3 \quad p_2(1+\rho) \quad p_3(1+\rho)]^{\mathrm{T}}. \tag{12}$$

These parameters are obtained using the usual least square formula

$$\theta = \left(\sum_{k=1}^{S} \Phi^{\mathrm{T}}(kT_s)\, \Phi\,(kT_s)^{\mathrm{T}} \right)^{-1} \sum_{k=1}^{S} \Phi^{\mathrm{T}}(kT_s)\, \phi(kT_s), \tag{13}$$

where T_s is the sample time (sufficiently small) and S is the number of samples of input–output data.

5. Experimental results

In the experimental set-up, angular positions of the pendulum and disk are measured with optical encoders with a resolution of 318.31 counts/rad (2000 counts/rev). Angular velocities and accelerations are obtained via an off-line numerical differentiation [16] of the position measures with a sample time of $T_s = 5$ ms.

5.1 Identification and Compensation of Friction at the Disk Joint

Since friction phenomenon at the disk bearing is relatively independent of the pendulum movement, the identification is performed with the pendulum fixed at the rest position ($q_1 = q_3 = 0$). Therefore, a reduced model for the motor–disk subsystem is

$$\dot{q}_4 = (1+\rho)(-p_2 q_4 + p_3 v - \tilde{\tau}_{\mathrm{dz}}). \tag{14}$$

To compensate the dead-zone friction term $\tilde{\tau}_{\mathrm{dz}}$ using the feedforward controller (7) with (8), the parameters v^+ and v^- must be identified. These parameters are obtained from the static input–output relationship between the uncompensated control input v and the steady-state velocity of the disk q_4. Figure 2(a) shows the experimental curve obtained by setting appropriate control input values, and recording the steady state velocity of the disk. The effect of the non-linear phenomenon can be interpreted as a large dead zone but this relation differs from that supposed in the dead-zone model (5) because of the discontinuity arising when the disk starts its motion. Nevertheless, an approximate value for v^+ and v^- can be obtained. A linear approximation of the straight part of the curve in figure 2(a) and a linear extrapolation suggest that a fairly good approximation of the dead-zone parameters is $v^+ \simeq v^- \simeq 31$. The compensation strategy (7) with (8) leads to the feedforward controller

$$v = u + v_{\mathrm{dz}} \operatorname{sgn} u,$$

with $v_{dz} = 31$. The experimental results obtained with this compensation scheme are shown in figure 2(b). Although the dead zone is not completely cancelled, a linear static relation between u and q_4 can be fitted with an error of 25 rad/s at $u = 15$ units. Using this feedforward compensation, the motor–disk model can be approximated by a linear model between input u and output q_4 with reasonable accuracy for $|u| > 20$. This range may be extended when the disk is in the dynamical regime.

To identify the parameters $p_2(1 + \rho)$ and $p_3(1 + \rho)$ of the dynamical model (14), it is assumed that an exact compensation for the dead-zone effect has been achieved. Then, the motor–disk subsystem can be modelled by

$$\dot{q}_4 = -p_2(1 + \rho)q_4 + p_3(1 + \rho)u.$$

Since the pendulum is fixed at rest, the original identification setup given by (10)–(12) is reduced to

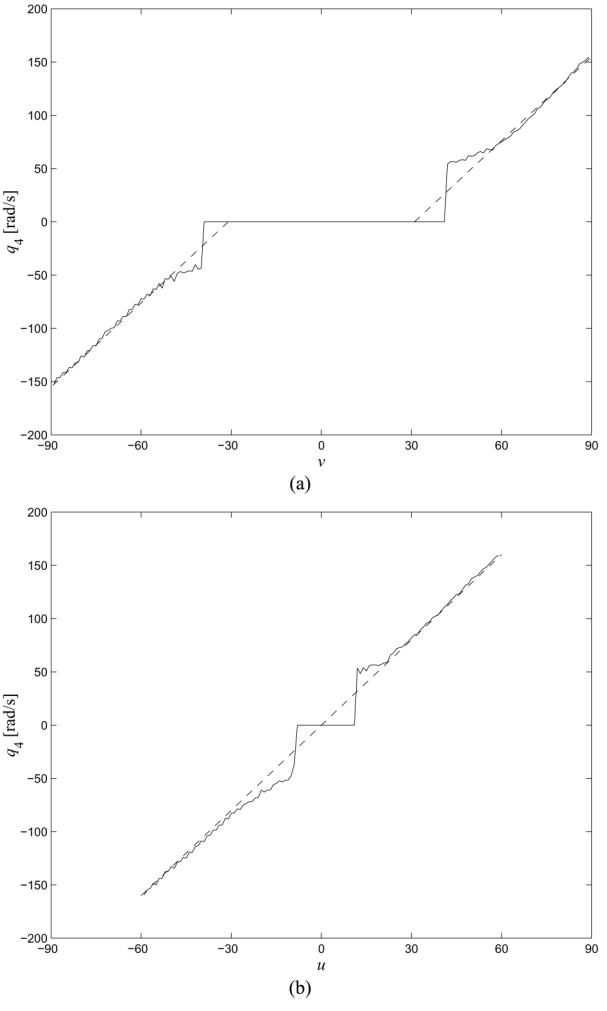

Figure 2. Dead-zone of the motor–disk subsystem. Static relationship between the angular velocity of the disk and the control input. (a) Response without compensation; (b) feedforward corrected response.

$$\phi^a = \dot{q}_4, \qquad \Phi^a = [\,-q_4 \quad u\,], \qquad \theta^a = [\,p_2(1+\rho) \quad p_3(1+\rho)\,]^{\mathrm{T}}.$$

The identification is performed by applying a 'chirp' input signal $u = 60 \sin[\omega(t)\, t]$, $\omega(t) = 3.2 + 1/75t$ (the natural frequency of the pendulum is approximately 5 rad/s) and $0 \leq t \leq 300$ ($S = 6 \times 10^4$ samples). The identified parameters are $p_2(1 + \rho) = 2.930$ and $p_3(1 + \rho) = 7.759$.

The quality of the model is evaluated comparing the experimental data and numerical simulations for sinusoidal input signals of different amplitudes. The frequency of the input signal is fixed at 5 rad/s (near to the natural frequency of oscillation of the pendulum) and the amplitude is set to 60 units (figure 3a), 40 units (figure 3b) and 20 units (figure 4a). The simulated disk velocity has a sinusoidal shape while the actual speed profile is a 'distorted' version of that, and the approximation is worst as the amplitude of the input decreases (see the corresponding errors e in figures 3a, 3b and 4a). Among other hypotheses, this behaviour can be related to a non-linear elastic characteristic of the rubber belt that couples the motor shaft with the disk.

Simplified analysis of the flexible coupling effect. The non-linear behaviour of the belt can be modelled assuming the position of the motor shaft as an additional generalized coordinate, and including a non-linear flexible joint. Then, the equation of motion (4b) translates to

$$\begin{aligned} I_2\,\ddot{q}_1 + I_2\,\ddot{q}_2 + b_2\,\dot{q}_2 + \Psi\left(q_2 - \frac{q_m}{N}\right) &= 0, \\ J_m\,\ddot{q}_m + b_m\,\dot{q}_m - \frac{1}{N}\Psi\left(q_2 - \frac{q_m}{N}\right) &= \tau_m, \end{aligned} \tag{15}$$

where $\Psi(\cdot)$ is a non-linear function representing the elastic behaviour of the rubber belt, q_m is the angular position of the motor shaft, J_m is the inertia of the motor, b_2 and b_m are viscous friction coefficients at the disk and motor joint, respectively, and τ_m is the motor torque (including the dead-zone feedforward compensation) given by

$$\tau_m = \frac{k_T}{R}\,V - \frac{k_T k_F}{R}\,\dot{q}_m\,.$$

Neglecting the inertia of the motor J_m, letting $\ddot{q}_1 = 0$ (the pendulum is fixed at rest position) and replacing $V = \beta u$, equations (15) reduce to

$$\begin{aligned} I_2\,\ddot{q}_2 + b_2\,\dot{q}_2 + \Psi\left(q_2 - \frac{q_m}{N}\right) &= 0, \\ \gamma\,\dot{q}_m - \frac{1}{N}\Psi\left(q_2 - \frac{q_m}{N}\right) &= \frac{k_T \beta}{R}\,u, \end{aligned}$$

where $\gamma := \left(N^2 k_T k_F / R\right) + b_m$.

The hypothesis of the non-linear behaviour of the rubber belt is validated by numerical simulations. The non-linear function $\Psi(\cdot)$ is approximated by the simple hysteresis function of figure 5 with fixed parameters k and d, although they probably depend on the velocity of the motor and disk joints. Since the angular position of the motor shaft of the experimental system is not measured, the parameters of this model cannot be obtained by the proposed identification procedure. For a small amplitude

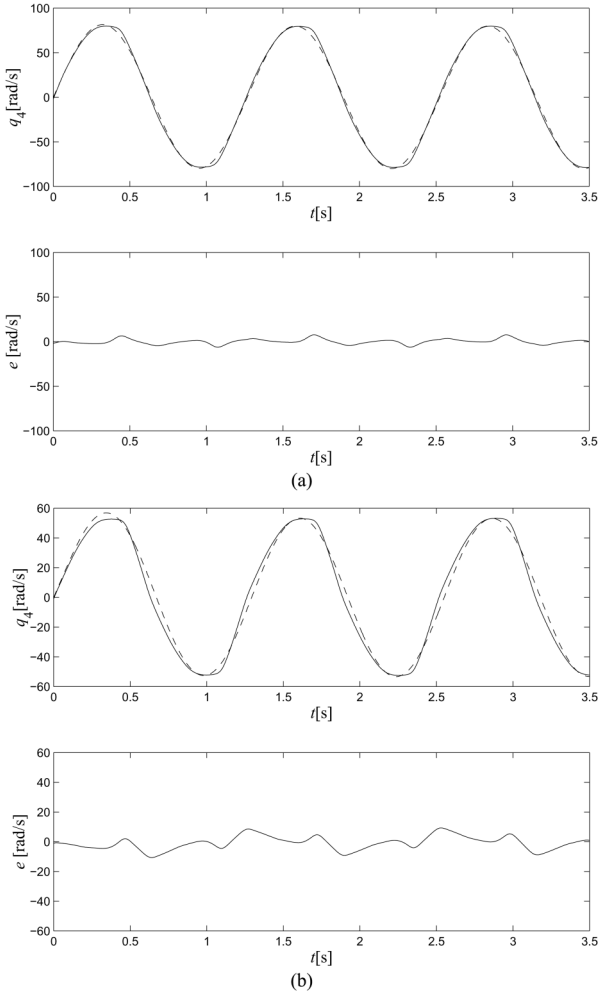

Figure 3. Numerical simulations and experimental data of the disk velocity, and the corresponding error using the dead-zone feedforward controller. The input signal is: (a) $u = 60 \sin(5t)$, (b) $u = 40 \sin(5t)$. (- -) Numerical simulation; (—) experimental data.

input $u = 20 \sin(5t)$, a fairly good approximation is obtained with parameter values $k/I_2 = 60\ \mathrm{s}^{-2}$, $d = 2$, $N = 13.5$ (measured), $b_2/I_2 = 10\ \mathrm{s}^{-1}$, $k/\gamma = 780\ \mathrm{s}^{-1}$ and $k_T\beta/(R\gamma) = 26\ \mathrm{s}^{-1}$, as revealed by the simulation results shown in figure 4(b). The identification error is reduced, and a closer matching with experimental data is obtained (compare with figure 4a).

Analysis of the Coulomb friction phenomenon. When including a Coulomb friction term, the model of the feedforward compensated motor–disk subsystem is given by

$$\dot{q}_4 = (1+\rho)(-p_2 q_4 + p_3 u - \tilde{\sigma}_{c2} \operatorname{sgn} q_4),$$

where $\tilde{\sigma}_{c2} := \sigma_{c2}/\hat{I}_1$. For estimating parameter $\tilde{\sigma}_{c2}(1+\rho)$, as well as $p_2(1+\rho)$ and $p_3(1+\rho)$, the identification setup given by (10)–(12) results in

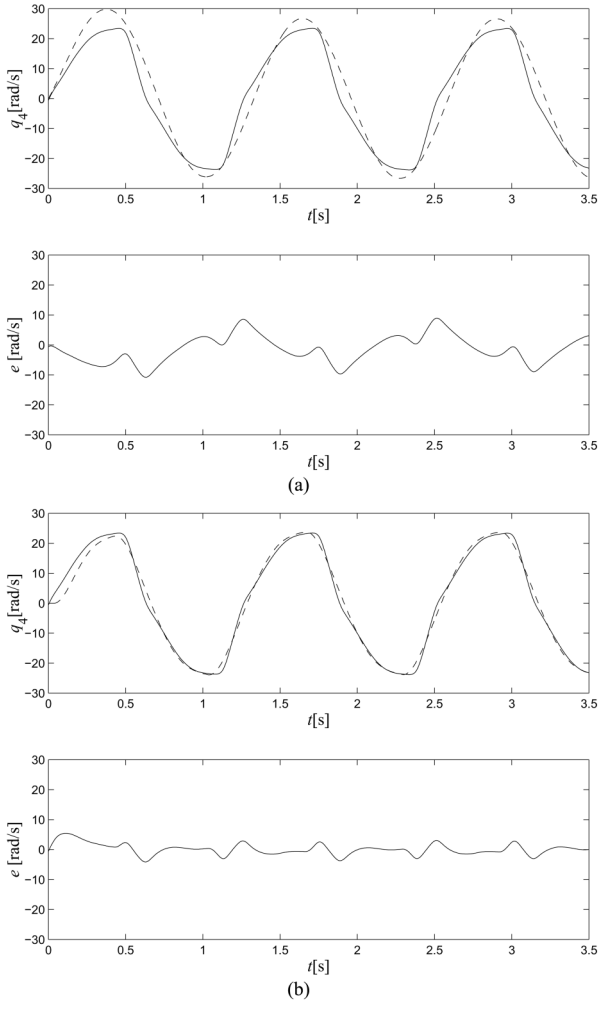

Figure 4. Numerical simulation and experimental data of the disk velocity, and the corresponding error using the dead-zone feedforward controller. Input signal $u = 20 \sin(5t)$. (a) Rigid coupling between the motor and the disk, (b) flexible coupling. (- -) Numerical simulation; (—) experimental data.

$$\phi^b = \dot{q}_4, \quad \Phi^b = [\,-q_4 \quad v \quad -\operatorname{sgn} q_4\,], \quad \theta^b = [\,p_2(1+\rho) \quad p_3(1+\rho) \quad \tilde{\sigma}_{c2}(1+\rho)\,]^{\mathrm{T}}.$$

The identification is performed applying the input signal $u = 60 \sin[\omega(t)\ t]$, $\omega(t) = 3.2 + 1/75t$, $0 \le t \le 300$. The identified parameters are $p_2(1+\rho) = 2.190$, $p_3(1+\rho) = 7.794$ and $\tilde{\sigma}_{c2}(1+\rho) = 40$. Notice that the parameter $p_3(1+\rho)$ is very close to the value obtained previously [$p_3(1+\rho) = 7.759$], but $p_2(1+\rho)$ has a rather lower value due to the neglected Coulomb friction term in the first model.

The accuracy of the identified model is analysed as before, by comparing experimental data with numerical simulations for sinusoidal inputs $u = A \sin(5t)$ of different amplitudes. For amplitudes $A = 60$ and $A = 40$ (figure 6(a) and (b), respectively) the results are very similar to those obtained neglecting the Coulomb friction term (compare with figure 3(a) and (b), respectively). For $A = 20$ (figure 7) the

approximation error is larger than that obtained without including Coulomb friction (compare with figure 4a). This fact validates the conjecture that Coulomb friction can be neglected from the model without degrading its predictive quality.

5.2 *Identification of the Complete Model*

The identification set-up for the dead-zone precompensated model is given by (13) with (10)–(12). By applying an input signal $u = 60 \sin [\omega(t)\, t]$, $\omega(t) = 3 + 1/100t$, $0 \leq t \leq 300$, the vector of parameters results in

$$\theta = [\,26.7594 \quad -2.7905 \quad 0.7620 \quad 0.0578 \quad 0.0054 \quad 0.0284 \quad 2.6060 \quad 7.1394\,]^{\mathrm{T}}. \quad (16)$$

The accuracy of the model prediction with the identified parameters is poor, as is revealed by performing a comparison between simulations and real data. Nevertheless, parameters $p_2(1 + \rho) = \theta_7 = 2.5194$ and $p_3(1 + \rho) = \theta_8 = 7.2813$ are relatively close to the values obtained before for the motor–disk subsystem.

To validate the parameters associated with the free pendulum ($\theta_1 - \theta_4$) an experiment setting free the pendulum at $q_1 = -1.422$ rad is carried out. The model of the free pendulum ($u = 0$) is given by

$$\dot{q}_3 = -p_1 \sin q_1 - \tilde{\sigma}_{a1} |\cos q_1| q_3 - \tilde{\sigma}_{v1}\, q_3 - \tilde{\sigma}_{b1}\, q_3^3,$$

and the reduced identification set-up is

$$\phi^c = \dot{q}_3, \quad \Phi^c = \left[\, -\sin q_1 \quad -|\cos q_1| q_3 \quad -q_3 \quad -q_3^3 \,\right], \quad \theta^c = [\,p_1 \quad \tilde{\sigma}_{a1} \quad \tilde{\sigma}_{v1} \quad \tilde{\sigma}_{b1}\,]^{\mathrm{T}}.$$

This results in $p_1 = 26.095$, $\tilde{\sigma}_{a1} = 0.003$, $\tilde{\sigma}_{v1} = 0.01$ and $\tilde{\sigma}_{b1} = 0.00047$. The simulation results obtained with the identified model are in a close agreement with the experimental data as shown in figure 8. This figure also reveals the low friction characteristic at the pendulum joint.

Notice that the four parameters (p_1, $\tilde{\sigma}_{a1}$, $\tilde{\sigma}_{v1}$ and $\tilde{\sigma}_{b1}$) are significantly far from the ones obtained with the complete system [$\theta_1 - \theta_4$ in (16)]. This result suggests that we

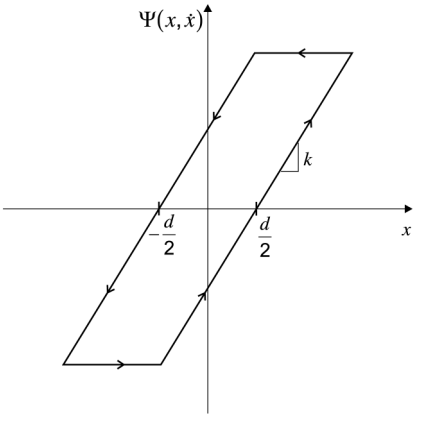

Figure 5. Hysteresis function used to model the non-linear behaviour of the rubber belt.

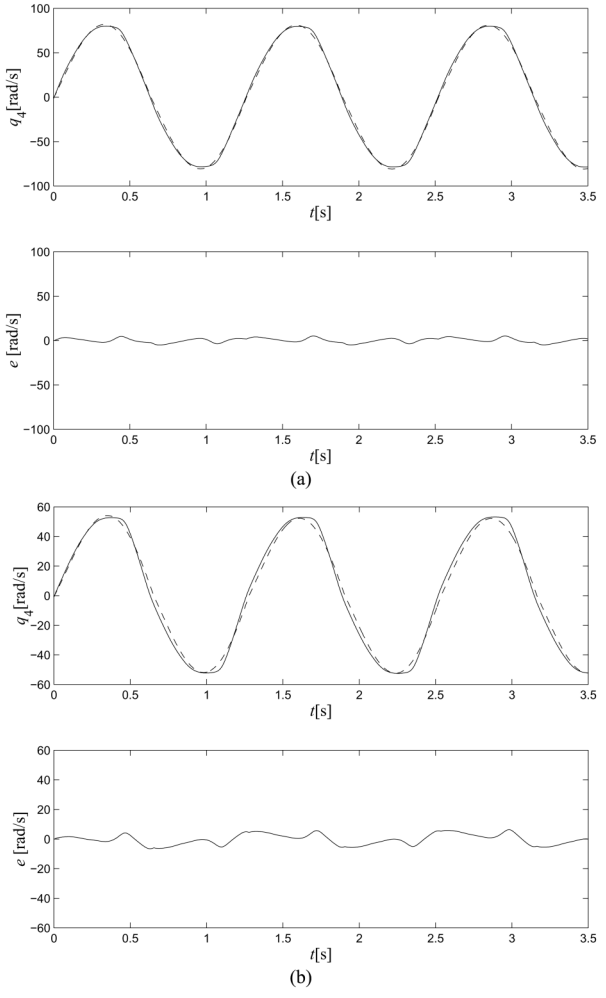

Figure 6. Numerical simulations and experimental data of the disk velocity, and the corresponding error, including Coulomb friction effects. The input signal is: (a) $u = 60 \sin(5t)$, (b) $u = 40 \sin(5t)$. (- -) Numerical simulation; (—) experimental data.

modify the identification set-up by reshaping ϕ, Φ and θ. The new set-up is obtained by eliminating parameters p_1, $\tilde{\sigma}_{a1}$, $\tilde{\sigma}_{b1}$ and $\tilde{\sigma}_{v1}$ from θ resulting in

$$\theta^d = [\, p_2 \quad p_3 \quad p_2(1+\rho) \quad p_3(1+\rho) \,]^{\mathrm{T}},$$

and considering

$$\Phi^d = \begin{bmatrix} q_4 & -u & 0 & 0 \\ 0 & 0 & -q_4 & u \end{bmatrix}, \qquad \phi^d = [\, \dot{q}_3 + \xi \quad \dot{q}_4 - \xi \,]^T,$$

where $\xi = p_1 \sin q_1 + \tilde{\sigma}_{a1} |\cos q_1| + \tilde{\sigma}_{v1} q_3 + \tilde{\sigma}_{b1} q_3^3$ is computed from experimental data and using parameter values identified with the free pendulum. By applying the input

signal $u = 60 \sin [\omega(t)t]$, $\omega(t) = 3 + 1/100t$, $0 \leq t \leq 300$, the redefined identification procedure gives

$$\theta^d = [\,0.0106 \quad 0.0286 \quad 2.6111 \quad 7.1395\,]^T.$$

The proposed structure for identification leads to a couple of possible values for the parameter ρ, since it may be obtained as $\rho_1 = \theta_3^d/\theta_1^d - 1 = 246.33$ or $\rho_2 = \theta_4^d/\theta_2^d - 1 = 249.63$. Nevertheless, both values are very close, validating these

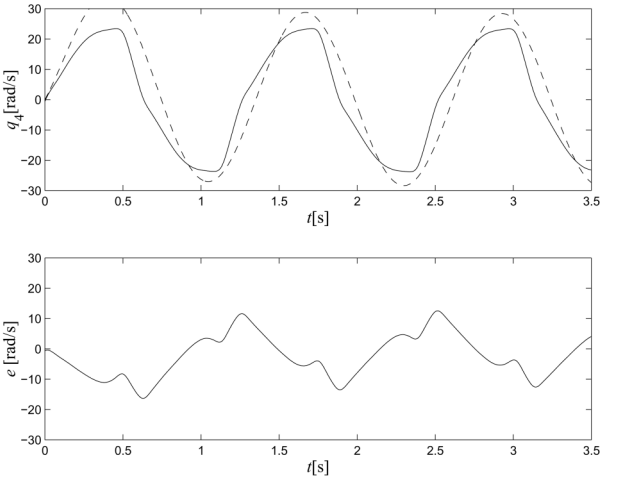

Figure 7. Numerical simulation and experimental data of the disk velocity, and the corresponding error, including Coulomb friction effects. The input signal is $u = 20 \sin (5t)$. (- -) Numerical simulation; (—) experimental data.

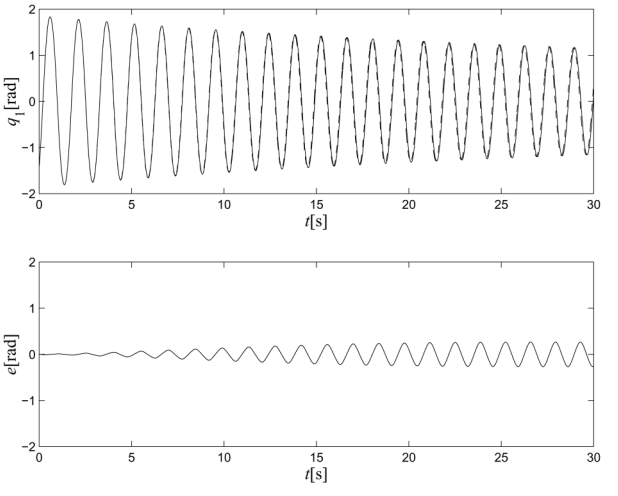

Figure 8. Numerical simulation and experimental data of the angular position of the pendulum, and the corresponding error, obtained setting free the pendulum at $q_1 = -1.442$ rad. (- -) Numerical simulation; (—) experimental data.

results. Hence, ρ is approximated by the averaged value $\rho = (\rho_1 + \rho_2)/2 = 247.24$. The full set of identified parameters is summarized in table 1.

Simulation results and experimental data of the complete system (9) are compared in figure 9(a). The simulated model is very close to the experimental data. The increment of the approximation error at high frequencies can be attributed to the long duration of the experiment and it is significantly reduced by restarting the simulation with the actual initial conditions, as shown in figure 9(b) for a restart time $t = 200$ s.

5.3 Validation of the Identified Model

In order to evaluate the model when the system performs oscillations of large amplitude a state feedback control law based on anticontrol of Hopf bifurcations is applied. As described in [15] it is possible to control the amplitude of the oscillation by means of the state feedback controller given by

$$u = k_1 q_3 + k_2 q_3^3.$$

This kind of amplitude control is useful for validation purposes because the desired amplitude of oscillation is obtained by properly choosing control gains k_1 and k_2 based on a bifurcation analysis and numerical continuation methods. Notice that the pendulum position is not directly used in the feedback law, and therefore a close response between the model and the actual system truly reveals the quality of the model.

For $k_1 = -10$ and $k_2 = 0.1$ the actual system performs an oscillation of amplitude $q_{1\max} \approx 2.58$ rad. Figure 10 shows the experimental data and the numerical simulation with parameter values given in table 1, revealing a very close matching.

6. Conclusions

Modelling and parameter identification of an inertia wheel pendulum benchmark has been addressed in this paper. Attention has been focused on deriving a simple but accurate model capable of reproducing large amplitude oscillations. It has been shown that the motor–disk subsystem presents a large dead zone which is modelled as an input voltage dependent friction torque. A viscous friction term is also included but Coulomb friction at this joint can be neglected without a noticeable degradation of the

Table 1. Parameter values.

Parameter	Values
p_1	26.0950
p_2	0.0106
p_3	0.0286
ρ	247.24
$\tilde{\sigma}_{a1}$	0.0030
$\tilde{\sigma}_{b1}$	0.0005
$\tilde{\sigma}_{v1}$	0.01

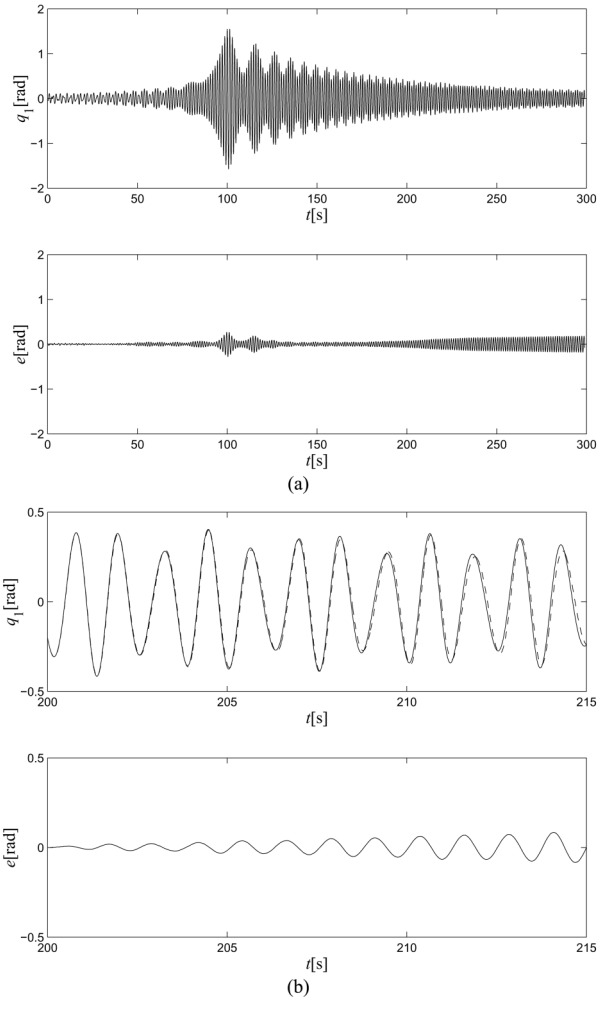

Figure 9. (a) Experimental data and error of the simulated model obtained with the chirp input signal $u = 60 \sin[\omega(t)\, t]$, $\omega(t) = 3 + 1/100t$, $0 \leq t \leq 300$. (b) Numerical simulation and experimental data, and error of the simulated model obtained by restarting the simulation and updating the initial conditions at $t = 200$ s of the original experience; (- -) Numerical simulation, (—) experimental data.

prediction quality of the identified model. A simple compensation scheme for the dead-zone effect has been proposed and a comparison between experimental data and numerical simulations for sinusoidal inputs of different amplitudes reveal an acceptable behaviour of the proposed model for the motor–disk subsystem. For low amplitude inputs the actual disk velocity presents a distorted sinusoidal shape and the error of the model approximation is increased. This phenomenon has been attributed to the non-linear elastic behaviour of the rubber belt coupling, and has been validated by simulations. The model of the dead-zone feedforward compensated system has been identified and the performance of the derived model has been analysed when the system develops large amplitude oscillations. A comparison between simulations and experimental data reveals very good accuracy of the identified model.

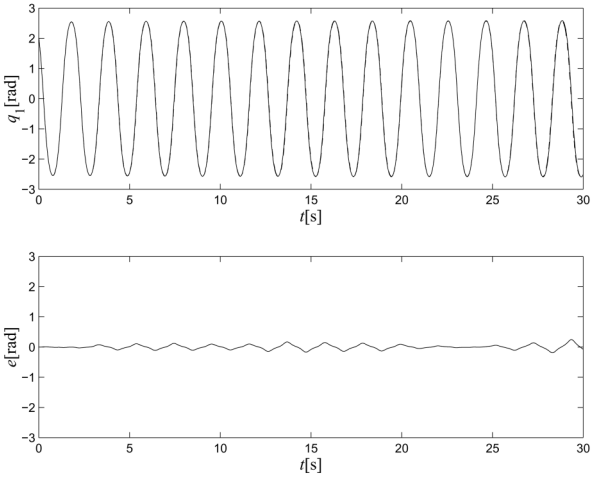

Figure 10. Large amplitude oscillations based on anticontrol of Hopf bifurcations: comparison of the closed-loop performance of the real system with numerical simulation. (- -) Numerical simulation; (—) experimental data.

ACKNOWLEDGEMENTS

This work is dedicated to the memory of our unforgettable friend Alfredo Desages, a mentor and pioneer in the field of non-linear systems analysis and control at the Universidad Nacional del Sur. This work was supported by the Universidad Nacional del Sur, the ANPCyT (PICT 11-12524) and CONICET.

References

[1] Lindskog, P. and Ljung, L., 1995, Tools for semiphysical modelling. *International Journal of Adaptive Control and Signal Processing*, **9**, 509–523.
[2] Goldstein, H., 1980, *Classical Mechanics* (Reading: Addison-Wesley).
[3] Armstrong-Hélouvry, B., Dupont, P. and Canudas de Wit, C., 1994, A survey of models, analysis tools and compensation methods for the control of machines with friction. *Automatica*, **30**, 1083–1138.
[4] Armstrong-Hélouvry, B., 1993, Stick slip and control in low-speed motion. *IEEE Transactions on Automatic Control*, **38**, 1483–1496.
[5] Hensen, R. H. A., van de Molengraft, M. J. G. and Steinbuch, M., 2003, Friction induced hunting limit cycles: a comparison between the Lugre and switch friction model. *Automatica*, **39**, 2131–2137.
[6] Olsson, H. and Åström, K. J., 2001, Friction generated limit cycles. *IEEE Transactions on Control Systems Technology*, **9**, 629–636.
[7] Canudas de Wit. C., Olsson, H., Åström, K. J. and Lischinsky, P., 1995, A new model for control of systems with friction. *IEEE Transactions on Automatic Control*, **40**, 419–425.
[8] Hirschorn, R. M. and Miller, G., 1999, Control of nonlinear systems with friction. *IEEE Transactions on Control Systems Technology*, **7**, 588–595.
[9] Spong, M. W., Corke, P. and Lozano, R., 2001, Nonlinear control of the reaction wheel pendulum. *Automatica*, **37**, 1845–1851.
[10] Praly, L., Ortega, R. and Kaliora, G., 2001, Stabilization of nonlinear systems via forwarding $mod\{L_gV\}$. *IEEE Transactions on Automatic Control*, **46**, 1461–1466.
[11] Olfati-Saber, R., 2001, Global stabilization of a flat underactuated system: The inertia wheel pendulum. In: *Proceedings of the 40th IEEE Conference on Decision and Control*, Orlando, USA, pp. 3764–3765.
[12] Alonso, D. M., Paolini, E. E. and Moiola J. L., 2002, Controlling an inverted pendulum with bounded controls. In: L. Gruene and F. Colonius (Eds) *Dynamics, Bifurcations, and Control*. LNCIS 273 (Berlin: Springer-Verlag), pp. 3–16.

[13] Ortega, R., Spong, M. W., Gómez-Stern, F. and Blankestein, G., 2002, Stabilization of a class of underactuated mechanical systems via interconnection and damping assignment. *IEEE Transactions on Automatic Control*, **47**, 1218–1233.
[14] Alonso, D. M., Berns, D. W., Paolini, E. E. and Moiola, J. L., 2003, Bifurcation control in feedback systems. In: G. Chen, D. J. Hill and X. Yu (Eds) *Bifurcation Control: Theory and Applications*. LNCIS 293 (Berlin: Springer-Verlag), pp. 205–228.
[15] Alonso, D. M., Paolini, E. E. and Moiola, J. L., 2001, Experimental application of the anticontrol of Hopf bifurcations. *International Journal of Bifurcation and Chaos*, **11**, 1977–1987.
[16] Lanczos, C., 1956, *Applied Analysis* (Englewood Cliffs: Prentice-Hall). Reprinted 1998 by Dover, New York.